AERODYNAMIC DESIGN MODIFICATION OF THE KOPTER AW09 HELICOPTER

Roman Reß (roman.ress@koptergroup.de), Maximilian Pulfer (maximilian.pulfer@koptergroup.de), Frieder Hirsch (frieder.hirsch@koptergroup.de), Kopter Germany GmbH, Altlaufstr.34, 85635 Höhenkirchen-Siegertsbrunn (Germany), Andreas Kümmel (andreas.kuemmel@tum.de), Christian Breitsamter (christian.breitsamter@aer.mw.tum.de), Chair of Aerodynamics and Fluidmechanics, Technical University of Munich, Boltzmannstr. 15, 85748 Garching (Germany)

Abstract
Wind tunnel testing and accompanying numerical analyses are the basic methods applied to improve and optimize the aerodynamic design of the Kopter AW09, a 2.8 ton-class single engine utility helicopter. In order to ensure good handling qualities and performance, modifications of the upper fuselage are tested and evaluated by means of force and moment measurements, particle image velocimetry, and CFD analysis. Based on particular examples, these methods are presented.

1. INTRODUCTION

As it is usually the case during the development phase of a completely new helicopter, the design of the Kopter AW09 goes through several stages of modifications and changes, some triggered by necessary installations of equipment and other requirements for aircraft systems, others by purely aerodynamic issues. To assist the evolution of the aerodynamic design, wind tunnel testing still plays an important role and is, in combination with CFD-analysis and flight test one of the key instruments for improving performance and handling. This paper presents selected results of wind tunnel experiments and a comparison with numerical analyses conducted during the development of the Kopter AW09.

2. EXPERIMENTAL SETUP

The present aerodynamic analysis is focused on the determination of the configuration's aerodynamic coefficients and the flow field topology in the wake of the upper fuselage. The experimental part of this analysis consists of force and moment measurements and flow field measurements by means of particle image velocimetry (PIV) in the wind tunnel.

2.1. Wind Tunnel

The experiments are conducted at the wind tunnel A of the Institute of Aerodynamics and Fluid Mechanics of the Technical University of Munich. This slow speed wind tunnel is of the closed return type, and has a test section dimension of 1.8m x 2.40m x 4.8m. It is capable of a maximum flow velocity of 65m/s when operating with an open test section. Figure 1 shows a schematic drawing of the tunnel.

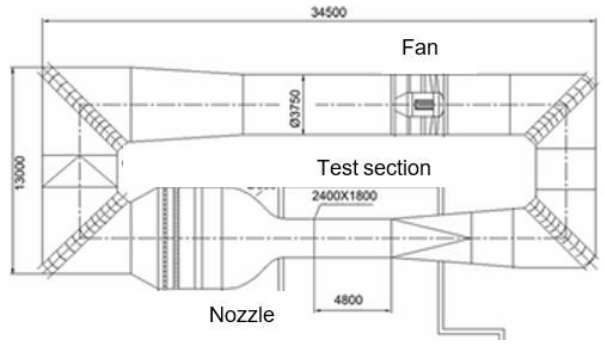

Figure 1: Slow speed wind tunnel A at the TUM [1]

2.2. Wind Tunnel Balance and Model Support

The force and moment measurements are performed using the wind tunnel A's 6-component underfloor balance and a tail sting support system running through the tail boom of the model (see [2]). The sting and the vertical part of the support structure are

completely faired in order to keep them free from aerodynamic loads (see Figure 2). The balance and the sting can be rotated to set angle of attack (AoA) and angle of sideslip (AoS) within a range of up to +/- 90 deg, as shown in Figure 3.

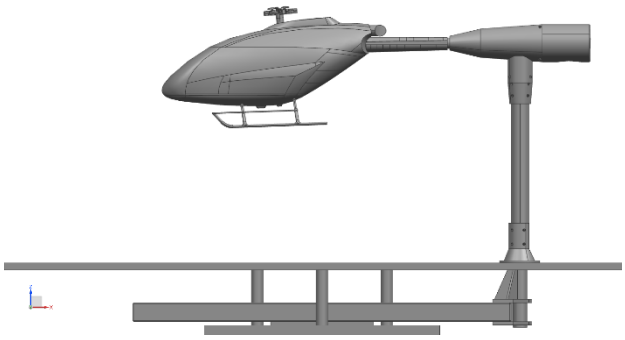

Figure 2: Model support system

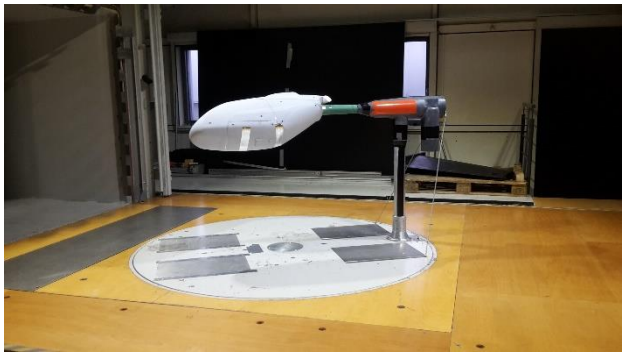

Figure 3: Rotating balance and sting to set AoA and AoS

2.3. Particle Image Velocimetry System

A Stereo-PIV system analyses the flow field in the wake of the fuselage by identifying magnitude and direction of the flow velocity in specifically defined planes within the zone of interest. In Figure 4 the PIV system is shown in the position used throughout the experiments on the left side of the wind tunnel test section. The system looks onto investigation planes in the wake of the helicopter fuselage. As the model can be rotated around the tail boom axis to any desired angle, investigation areas in the wake of the sides and the lower aft body of the fuselage can be analysed without having to move and readjust the camera system. While performing experiments with rotating rotor head, the PIV can be triggered by a predefined azimuth (Ψ) position of the rotor head with the recording rate adapted to the rotor head speed and recurring rotor head positions.

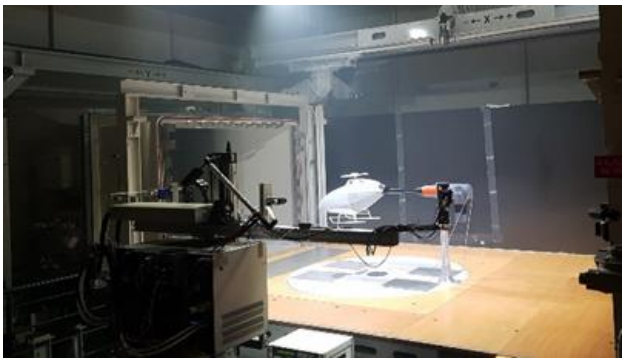

Figure 4: Stereo-PIV at the wind tunnel test section

2.4. Wind Tunnel Model

The 1:6.5 scale wind tunnel model comprises fuselage, landing gear, rotor head, and a truncated tail boom. Optionally, a full tail boom including horizontal stabilizers and fin can be attached. Provision is made to drive the rotor head with a 400W electric motor. The model's body work consists of exchangeable segments, forming the front part of the fuselage, the upper fuselage including mast fairing, the lower aft body, and the belly. Different versions of landing gears and rotor heads can be attached. The present analysis focuses on early to intermediate development stages during the evolution of the upper fuselage and cowling design. As an example, two development configurations, the baseline version as shown in Figure 5, and a modified variant (depicted in Figure 6) are analysed. The modified shape, coming along with a slightly extended rotor mast, features a considerably more streamlined fuselage - tail boom connection, and a distinctive mast fairing. In addition, the landing gear attachment is slightly changed with the rear cross tube being positioned somewhat lower than on the baseline variant.

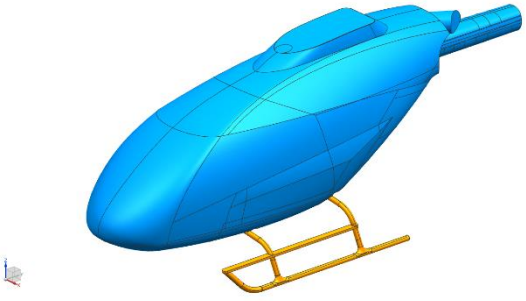

Figure 5: Baseline configuration

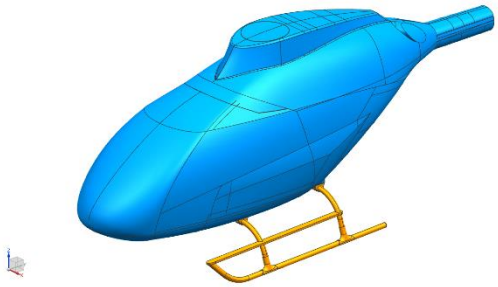

Figure 6: Modified configuration

2.5. Test Parameters

The wind tunnel experiments presented here are run with a free stream velocity of 40 m/s yielding a Reynolds number of about 800000. Cases including the rotating rotor head are performed with the rotor speed set to an advance ratio of 0.34. The flow field analysis comprises up to four investigation planes in the wake of the fuselage, (see Figure 9). For several test cases, additional planes are chosen at the left, the right, and below the tail boom. The PIV investigation presented here is performed at AoA = 0 deg and AoS = 0 deg, and the results of this paper are generated with the model having the truncated tail boom installed. The PIV system operates at a rate of 13.87Hz. The rate is chosen to capture the flow field with the rotor head (and the truncated blades) at the same azimuth position for each sample, by taking into account the maximum operating rate of the laser system. In general, two series of recordings are taken, one with a blade over the tail boom, and another series with a blade over the nose of the helicopter.

3. NUMERICAL ANALYSIS

During the development phase, numerous CFD calculations regarding all parts and aspects of the helicopter and its operation are performed. Here, the principal setup used to create the numerical data is provided. All meshing and computational tasks are performed using the Siemens Simcenter STAR-CCM+ software [3].

3.1. Mesh

For the numerical investigation of all configurations, a spherical domain is applied and the helicopter model is placed in its centre (see Figure 7). The diameter of the sphere is approximately 33 times the length of the helicopter simulation model. Solely unstructured meshes are generated and the meshes consist mainly of polyhedral cells. Prism layers are created on the walls to account for the boundary layer. A y+ value < 1 is achieved in most regions. In areas of significant flow gradients the mesh is refined accordingly.

In order to include the effect of a rotating main rotor head in the analysis of specific configurations, the overset mesh technique [5] is applied for the corresponding simulation cases. Therefore, the setup is split up into a rotating rotor head domain and a fixed spherical outer domain, which represents the far field and contains the non-rotating parts of the helicopter. In the area of the main rotor head and its predicted wake, the mesh is refined. This ensures to capture the flow topology around the tail boom for the comparison with wind tunnel PIV data. The meshing parameters are chosen to match the cell sizes in the overset region of both domains. This guarantees a similar resolution of data points for the interpolation in the area where the rotating and non-rotating domains overlap.

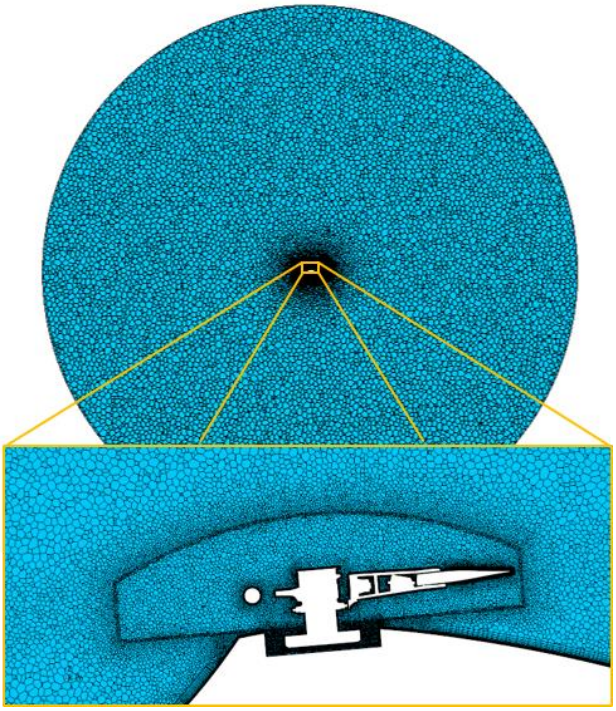

Figure 7: Section of simulation domain and detail view of overset mesh for rotating main rotor head simulations

For the CFD simulations the main rotor blades are truncated at the same radial station as for the wind tunnel model. An illustration of the simplified main rotor head model with blade stubs applied in the numerical investigation is shown in Figure 8.

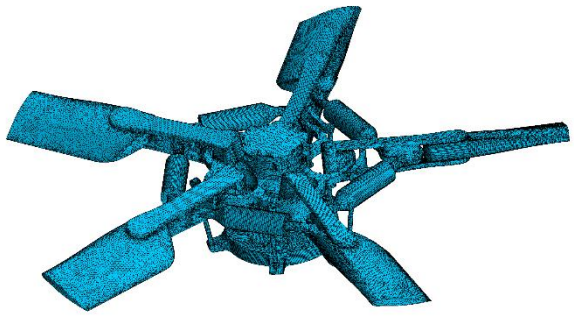

Figure 8: Model of rotating main rotor head used for numerical investigation

3.2. Setup and Solver

The outer boundary of the far field has the shape of a sphere and is defined as freestream inlet/outlet. The full-scale Reynolds numbers of the real helicopter as well as the wind tunnel model-scale Reynolds numbers are considered for the numerical investigation.
The Unsteady Reynolds-Averaged Navier-Stokes equations (URANS) are solved by an implicit unsteady solver regarding a coupled flow method. A first order discretization scheme is applied. As turbulence model, the SST Menter k-ω model [4] is employed. For the simulation cases considering the rotating main rotor head, the discretization scheme is changed to a second order scheme. The collective pitch angle setting of the main rotor stubs is defined in accordance with the main rotor model used in the experimental investigation. The rotational speed of the rotor is specified properly to match the setup of the wind tunnel measurements. The time step is adjusted to an equivalent of $\Delta\Psi$ = 2 deg of main rotor rotation for the first five rotations. Subsequently, the time step is reduced to meet an angular step width of $\Delta\Psi$ = 1 deg. This allows an accurate temporal resolution of the main rotor wake. With the smaller time step, another two full main rotor rotations are computed before the data for the flow visualization in the area of the tail boom is evaluated. The sections for the extraction of the numerical data are placed at the same longitudinal positions as the PIV measurement planes.

4. RESULTS

In order to evaluate the different methods, results of the wind tunnel experiments and CFD calculations are compared by looking at the flow field data and the resulting aerodynamic coefficients of the configurations.

4.1. Flow Field

Examining the flow field in the wake of the fuselage, results of the PIV investigation are presented with a focus on the wake of the upper fuselage, where the shape modifications are expected to show a significant effect. Figure 9 shows the positions of the investigation planes chosen for the PIV measurement of the wake flow. During the described experiments, the tail boom is truncated at the position of investigation plane 1 (P1).

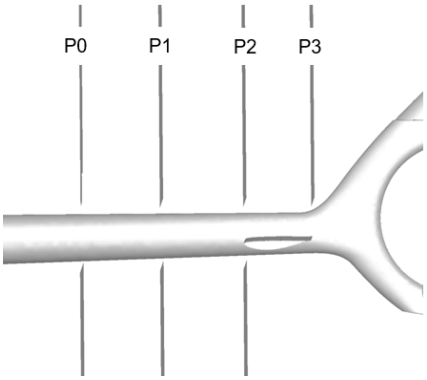

Figure 9: Investigation planes P0 - P3 along the tailboom

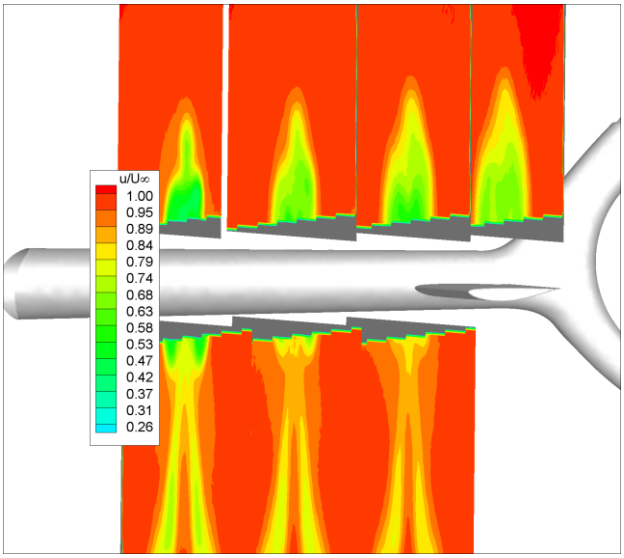

Figure 10: Axial flow velocity u/U_∞, baseline configuration, AoA, AoS = 0 deg

Figure 10 and Figure 11 show the axial flow velocity u/U_∞ as coloured contour plots in all planes along the tail boom, giving a good overview of the flow field in the wake of the fuselage. In Figure 10 - Figure 11, the full tail boom geometry is shown only to illustrate the position of the planes relative to the helicopter fuselage. Looking at Figure 10, the baseline configuration causes a significant deceleration of the axial flow and a considerably disturbed airflow in a large volume, easily reaching the helicopter's fin and

shroud. These effects are expected to cause difficult flow conditions in the region of the control surfaces and around the tail rotor. In addition, the large volume of decelerated flow points to a significant source of drag. By contrast, the modified configuration (Figure 11) clearly establishes a less turbulent flow field in the wake of the upper fuselage. The modification also shows a noticeable downward directing effect, thus not only leading to reduced drag, but also augmenting lift.

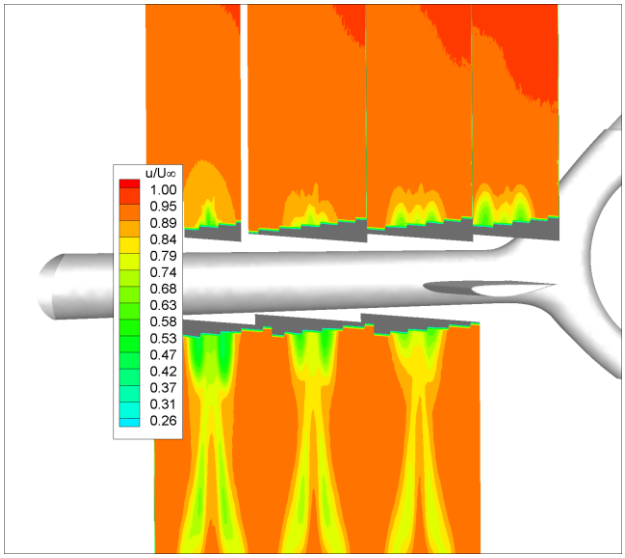

Figure 11: Axial flow velocity u/U∞, modified configuration, AoA, AoS = 0 deg

Figure 12 for the baseline variant, and Figure 13 for the modified variant, allow for a closer look into investigation plane 3, positioned directly in front of the vertical fin.

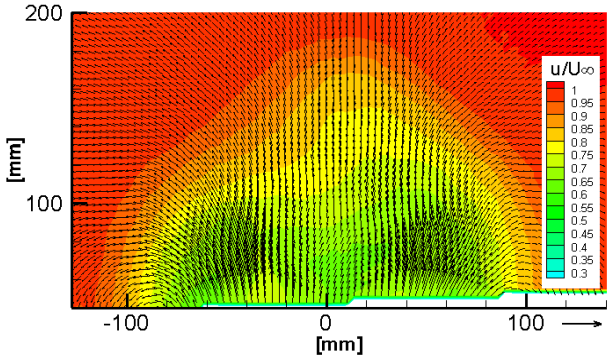

Figure 12: Flow field in plane 3, baseline configuration

Apart from the axial velocity u/U∞ as coloured contours, the plots contain the in-plane velocities as vectors and confirm the greatly reduced perturbation of the flow in front of the vertical fin.

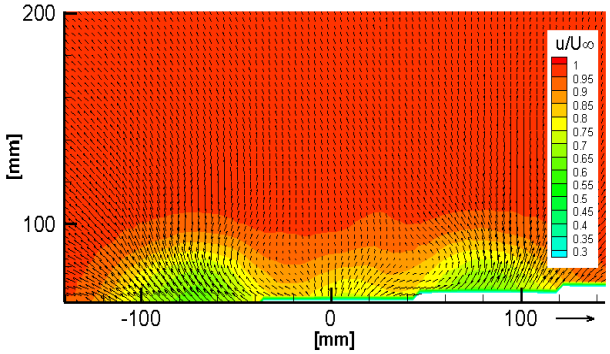

Figure 13: Flow field in plane 3, modified configuration

Also, note the much-reduced upward component of the in-plane velocity, which should go along with increased lift. This will be examined in the next section, which presents results of the wind tunnel balance measurements and numerical analyses in form of aerodynamic coefficients.

4.2. Aerodynamic Coefficients

On the basis of the previous example, aerodynamic coefficients of the two variants are compared in Figure 14 - Figure 17. The modification leads to a considerable drag reduction in the order of 10 - 15% in the negative AoA range, and still to a slight drag reduction up to +5 deg (see Figure 14), thus being very effective within the AoA-range most relevant for improvements of the flight performance. Figure 15 proves, that this drag reduction is also noticeable throughout an AoS range of -12 to +12 deg (at 0 deg AoA). Noteworthy is, that this drag reduction is achieved despite the modified landing gear attachment, which alone is expected to cause an increase in drag.

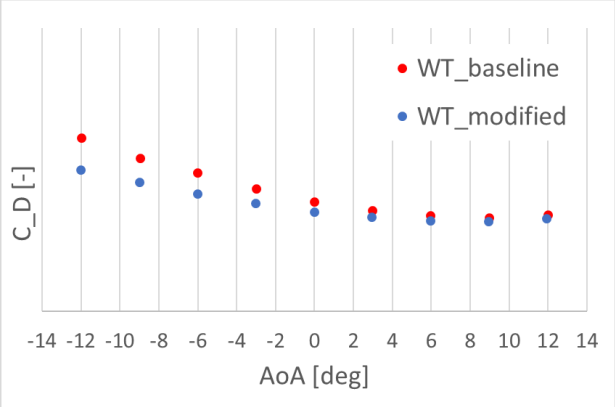

Figure 14: Drag coefficient vs AoA, AoS = 0 deg

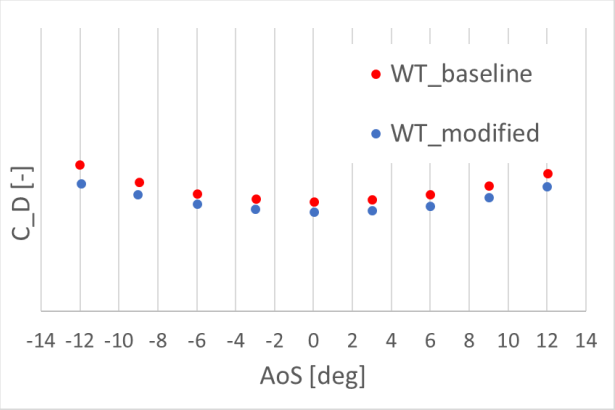

Figure 15: Drag coefficient vs AoS, AoA = 0 deg

The analysis of the flow field already indicated a further benefit of the modification, which becomes evident in Figure 16 and Figure 17. The lift coefficient of the modified variant is greater than the baseline's over a wide range of AoA, in particular at negative AoA. The shape modification with its much smoother and streamlined upper fuselage expectedly shows less drag and an increased lift/reduced down force in the balance measurements. This also remains valid at small and medium angles of sideslip (at AoA = 0 deg), as can be seen in Figure 17.

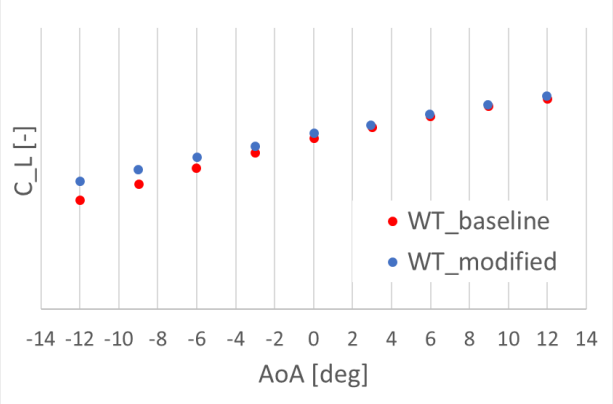

Figure 16: Lift coefficient vs AoA, AoS = 0 deg

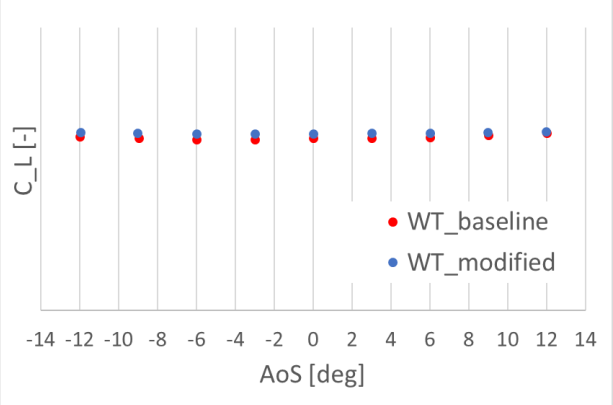

Figure 17: Lift coefficient vs AoS, AoA = 0 deg

Concluding at this point, the results of the balance measurements suit the flow field analyses quite well and confirm the expected benefits of the shape modification and the adequacy of the applied methods.

To further examine the aerodynamic characteristics of the configurations, appropriate comparisons and a matching of the methods of analysis is important. A fundamental criterion for the quality of simulation methods in aerodynamics is the similarity of the flow field topology. In order to examine this in a more detailed way, the following section compares results of the particle image velocimetry measurements performed in the wind tunnel, with correlated CFD analyses. As an example, the modified configuration is selected and, for this purpose equipped with a rotating rotor head. In general, the PIV experiments with a rotating rotor head are aimed at investigating the path of the highly turbulent wake flow of the rotor head in order to find possibilities for redirecting it away from important control surfaces such as stabilizers, fin, and the shrouded tail rotor.

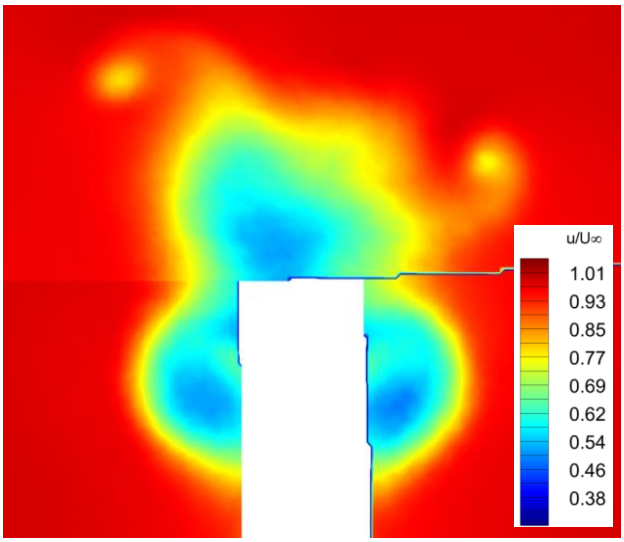

Figure 18: Axial flow velocity u/U∞ in plane 1, PIV

Figure 18 shows the axial flow velocity u/U∞ in plane 1 as a coloured contour plot. The vortices shed by the tips of the rotating rotor head are clearly resolved. In addition, conical vortices originating from the fuselage's lower aft body can be detected on the lower left and right sides of the tail boom as blue areas of reduced axial velocity. For a detailed description of the types of flow related to the rear fuselage upsweep, see [6]. Above the tail boom, the wake of the rotor hub is clearly distinguishable as an area of reduced velocity.

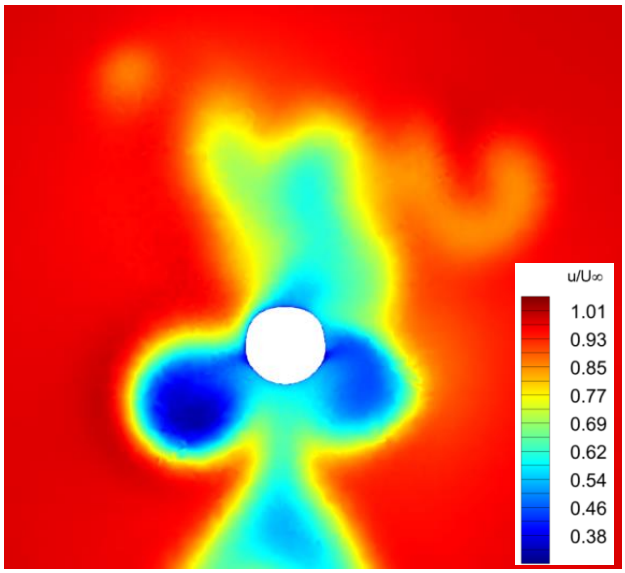

Figure 19: Axial flow velocity u/U_∞ in plane 1, CFD

Comparing it with Figure 19, the result of a corresponding CFD calculation shows a very similar flow topology. The CFD computation reproduces the vortices and their positions with respect to the tail boom very well. The regions of decelerated flow have slightly different dimensions and positions, but altogether closely resemble the PIV picture.

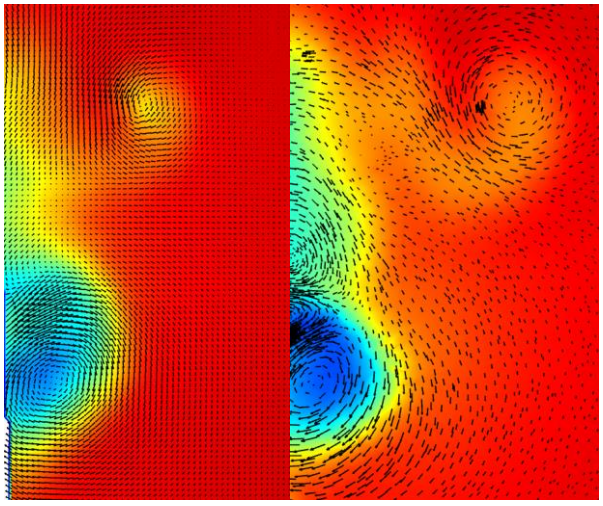

Figure 20: In-plane velocity as vectors in plane 1, PIV (left), CFD (right)

Figure 20 shows in a more detailed view of plane 1 the in-plane velocity vectors at the port side of the tail boom. The tip vortex of the blade stub is captured by both methods, as well as the dominant vortex next to the tail boom. The CFD result indicates another small vortex slightly above the tail boom, which is not distinctively present in the PIV picture.

As a conclusion concerning the flow field topology, the analysis shows generally a good agreement of PIV and CFD in the wake of the rotor head with some minor discrepancies. In order to examine, whether the flow field similarity shown by PIV and CFD also leads to similar aerodynamic forces, a comparison of the resulting aerodynamic coefficients from CFD computations and balance measurements are plotted in Figure 21 - Figure 24. In Figure 21, the measured drag coefficient vs AoA of the modified configuration is plotted against a CFD result. CFD and wind tunnel result match quite well at small to medium positive angles of attack. At negative angles of attack, the measurement result and the CFD result diverge in a way, that CFD predicts lower drag than measured in the wind tunnel. This becomes even more dominant at higher negative angles of attack.

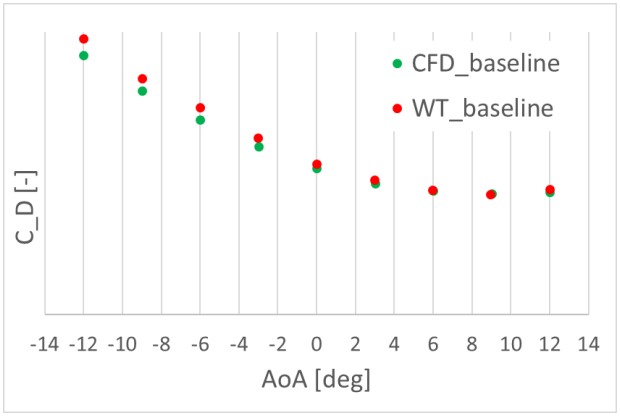

Figure 21: WT-CFD comparison, drag coefficient vs AoA, AoS = 0 deg, baseline configuration

Figure 22 shows the drag coefficient with respect to angle of sideslip (AoA = 0 deg). The numerically determined drag coefficient remains lower for all shown angles of sideslip and in addition, an asymmetry in the difference between CFD and wind tunnel measurement becomes evident, which can be explained by the exhaust pipe. Obviously, it causes different flow phenomena locally, which can have an effect on a larger scale.

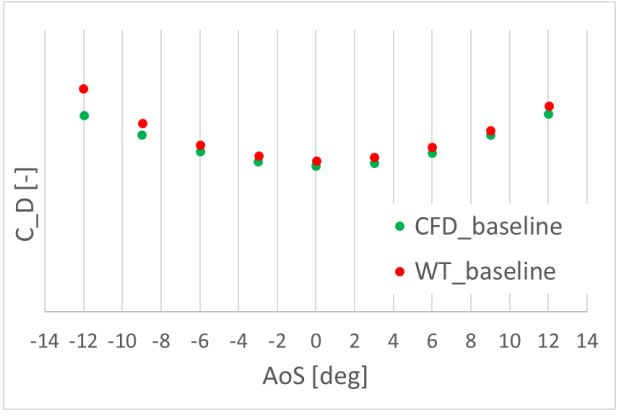

Figure 22: WT-CFD comparison, drag coefficient vs AoS, AoA = 0 deg, baseline configuration

The lift coefficient (Figure 23) shows a correlated behaviour, as the CFD result indicates less lift/down force at higher positive/negative angles of attack than the balance measurement. Within the AoS-range shown in Figure 24, the numerically determined lift coefficient is also smaller than the measured lift coefficient. Here again is a slight asymmetry noticeable. The difference between CFD calculation and balance measurement increases with positive angles of sideslip. As already mentioned, the only asymmetry in the geometry is the exhaust pipe at the backside of the upper fuselage, which obviously implicates different flow phenomena.

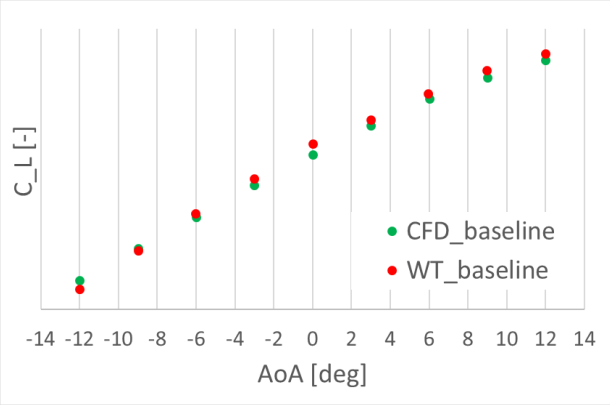

Figure 23: WT-CFD comparison, lift coefficient vs AoA, AoS = 0 deg, baseline configuration

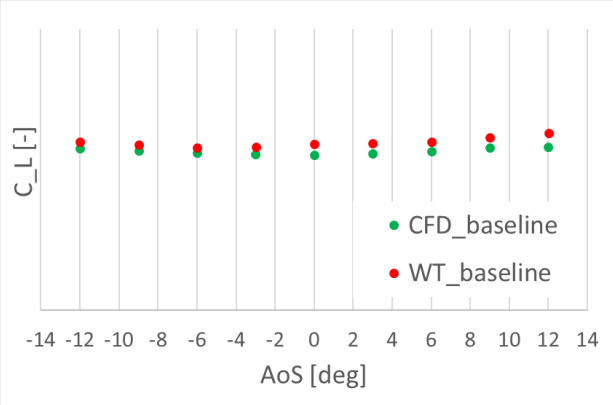

Figure 24: WT-CFD comparison, lift coefficient vs AoS, AoA = 0 deg, baseline configuration

To complete this short tour through the experimental and numerical analyses, the drag reduction of the fuselage modification, as predicted by CFD and measured in the wind tunnel is shown in Figure 25. The CFD analysis predicts a slightly higher drag reduction than measured in the wind tunnel. There is a larger difference between CFD result and experimental result for the modified configuration, which is with its smoothened shape more prone and sensitive to varying characteristics of flow separation.

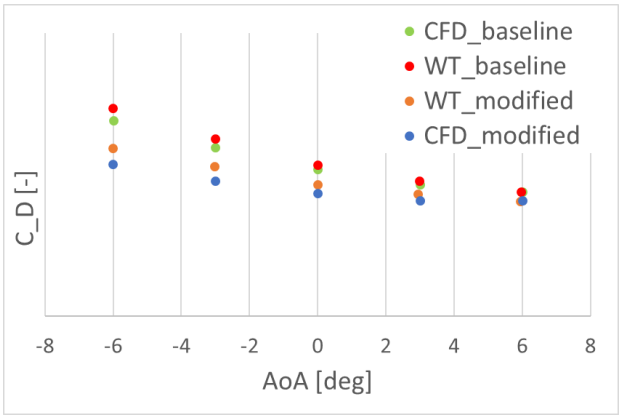

Figure 25: Drag coefficient vs AoA, AoS = 0 deg

To summarise the analyses, all applied investigation methods predicted an improved aerodynamic performance of the design modification with respect to the baseline variant and motivate an incorporation into the design.

5. OUTLOOK

The results of the wind tunnel campaign and the corresponding CFD analysis confirm the expected benefits of this particular design modification during the development phase of the Kopter AW09. As these results marked a considerable advance in terms of efficiency and handling characteristics, further and more detailed optimisation of the helicopter fuselage followed. Wind tunnel investigations, as described in the present paper form an invaluable contribution to support various development and design activities of the AW09 helicopter. The wind tunnel model and derived versions of it with adapted instrumentation is continuously in use to support aerodynamic analyses of the AW09 and contributes to the optimisation of the design. Combining wind tunnel tests, numerical analyses and finally, flight test still provide the basis for a successful development of the aerodynamic characteristics of a helicopter.

REFERENCES

[1] Chair of Aerodynamics and Fluidmechanics, Technical University of Munich, Boltzmannstr. 15, 85748 Garching (Germany)

[2] Vogel F, Breitsamter C and Adams N A. Aerodynamic Investigations on a Helicopter Fuselage, Proceedings of the 29th AIAA Applied Aerodynamics Conference, Honolulu, HI 2011.

[3] Siemens Simcenter STAR-CCM+ User Guide version 2021.1

[4] Menter F. R., Two equations eddy viscosity turbulence models for engineerings applications, AIAA journal, Vol. 32, pp. 1598-1605, 1994

[5] Benek, J.; Steger, J. L.; Dougherty, F. C.: A Flexible Grid Embedding Technique with Application to the Euler Equations. AIAA Paper 83-1944, 1983

[6] Seddon, Basic Helicopter Aerodynamics, BSP PROFESSIONAL BOOKS London, 1990, p 83.